submitted to the **Journal of Chemical Physics,** ***September 8, 2005***

Mean Field Dynamics with Stochastic Decoherence (MF-SD): A New Algorithm for Nonadiabatic Mixed Quantum/Classical Molecular Dynamics Simulations with Nuclear-Induced Decoherence

Michael J. Bedard-Hearn, Ross E. Larsen, Benjamin J. Schwartz*

Department of Chemistry and Biochemistry
University of California, Los Angeles
607 Charles E. Young Dr. East
Los Angeles, CA 90095-1569

Abstract: They key factors that distinguish algorithms for nonadiabatic mixed quantum/classical (MQC) simulations from each other is how they incorporate quantum decoherence – the fact that classical nuclei must eventually cause a quantum superposition state to collapse into a pure state – and how they model the effects of decoherence on the quantum and classical subsystems. Most algorithms use distinct mechanisms for modeling nonadiabatic transitions between pure quantum basis states ("surface hops") and for calculating the loss of quantum mechanical phase information (e.g., the decay of the off-diagonal elements of the density matrix). In our view, however, both processes should be unified in a single description of decoherence. In this paper, we start from the density matrix of the total system and use the frozen Gaussian approximation for the nuclear wave function to derive a nuclear-induced decoherence rate for the electronic degrees of freedom. We then use this decoherence rate as the basis for a new nonadiabatic MQC molecular dynamics (MD) algorithm, which we call mean-field dynamics with stochastic decoherence (MF-SD). MF-SD begins by evolving the quantum subsystem according to the time-dependent Schrödinger equation, leading to mean-field dynamics. MF-SD then uses the nuclear-induced decoherence rate to determine stochastically at each time step whether the system remains in a coherent mixed state or decoheres. Once it is determined that the system should decohere, the quantum subsystem undergoes an instantaneous total wave function collapse onto one of the adiabatic basis states and the classical velocities are adjusted to conserve energy. Thus, MF-SD combines "surface hops" and decoherence into a single idea: decoherence in MF-SD does not require the artificial introduction of reference states, auxiliary trajectories or trajectory swarms, which also makes MF-SD much more computationally efficient than other nonadiabatic MQC MD algorithms. The unified definition of decoherence in MF-SD requires only a single *ad hoc* parameter, which is not adjustable but instead is determined by the spatial extent of the nonadiabatic coupling. We use MF-SD to solve a series of one-dimensional scattering problems and find that MF-SD is as quantitatively accurate as several existing nonadiabatic MQC MD algorithms, and significantly more accurate for some problems.

*Corresponding author. Voice: (310) 206-4113; Fax: (310) 206-4038; e-mail: schwartz@chem.ucla.edu

I. Introduction

One of the interesting features that distinguishes condensed-phase chemical reactivity from that in the gas phase is that condensed-phase systems often show strong coupling between solute electronic states due to nonadiabatic effects induced by motions of the solvent. This breakdown of the Born-Oppenheimer approximation means that quantum mechanical dynamics must be governed by the time-dependent Schrödinger equation (TDSE), which is unfortunate because fully quantum mechanical calculations that would allow us to understand the dynamics of such condensed-phase systems are not yet computationally feasible. This makes it desirable to develop computational strategies that eliminate as many of the quantum mechanical degrees of freedom as possible without sacrificing information about the physics of interest. The most common approach lies in mixed quantum classical (MQC) simulations, which treat most of the particles classically but maintain quantum information about important degrees of freedom such as the valence electrons or relevant vibrational modes of a solute engaged in a chemical reaction (throughout this paper, we will interchangably refer to quantum degrees of freedom as "electronic" and also refer to classical degrees of freedom as "nuclear" without loss of generality). To this end, several MQC molecular dynamics (MD) algorithms for studying condensed-phase nonadiabatic dynamics have been developed over the last 15 years.[1–11]

If the entire system (bath included) were treated quantum mechanically, then dynamics calculated via the time-dependent Schrödinger equation would be exact. However, the presence of classical particles induces nonadiabatic coupling that causes the TDSE to evolve pure wave functions into quantum mechanical superpositions, which are inherently incompatible with classical mechanics: mixed quantum states produce unphysical dynamics for the classical particles, leading to apparent paradoxes such as "Schrödinger's Cat".[12] Thus, in the asymptotic limit, only pure quantum states are consistent with the presence of classical particles. The act of collapsing a quantum superposition state to a pure state is often viewed as a "measurement" of the quantum subsystem by the classical subsystem; the measurement resolves the superposition into a pure state, and the classical particles play the role of the observer. The fact that the presence of classical particles must eventually cause reduction of the quantum wave function to a pure state is known as quantum *decoherence*; von Neumann has pointed out that decoherence is not time-reversible,[13] and Zurek has argued that decoherence is caused only by the interaction of a quantum superposition with a classical observer.[14] How exactly this process is introduced at the boundary of classical and quantum mechanics is the key question facing nonadiabatic MQC methods, which fundamentally rely on co-existing quantum and classical subsystems.

Although we know of no formal way to derive decoherence from the TDSE, we can justify why the classical degrees of freedom are what controls quantum decoherence. If we assume that the total

system wave function at time t, $|\Psi(t)\rangle$, can be written as a product of time-dependent nuclear, $|\chi(t)\rangle$, and electronic, $|\psi(t)\rangle$, wave functions, and that the electronic wave function $|\psi(t)\rangle = \sum_j c_j(t)|\phi_j(t)\rangle$ can be written as a linear combination of basis states $\{|\phi_j\rangle\}$, then the total density matrix, $\hat{\rho}(t)$, is

$$\begin{aligned}\hat{\rho}(t) &= |\Psi(t)\rangle\langle\Psi(t)| = |\psi(t)\rangle\langle\psi(t)| \times |\chi(t)\rangle\langle\chi(t)| \\ &= \sum_{j,j'} \left(c^*_{j'}(t) c_j(t) |\phi_j\rangle\langle\phi_{j'}| \right) \times \left(|\chi(t)\rangle\langle\chi(t)| \right) . \end{aligned} \tag{1}$$

The information about the relative phase (coherence) between different basis states is contained in the off-diagonal ($k \neq k'$) elements of the total density matrix,[15]

$$\rho_{k,k'}(t) = c^*_{k'}(t) c_k(t) \times \langle \chi_k(t) | \chi(t) \rangle \langle \chi(t) | \chi_{k'}(t) \rangle \equiv \rho_{k,k'}(t) \times D_k(t) D^*_{k'}(t), \tag{2}$$

where $\rho_{k,k'}(t) = c^*_{k'}(t) c_k(t)$ is an element of the *electronic* density matrix at time t, $|\chi_k(t)\rangle$ is the nuclear wave function associated with the electronic basis state $|\phi_k\rangle$ at time t, and we call the inner product $D_k(t) = \langle\chi_k(t)|\chi(t)\rangle$ (and its complex conjugate, $D^*_{k'}(t)$) the *decoherence function*.[16] Phase information (coherence) is lost whenever any of the $\rho_{k,k'}(t) = 0$, and Eqn. 2 shows that this can result either from electronic dynamics, when $\rho_{k,k'}(t)$ decays to zero, or from nuclear dynamics, when the decoherence function $D_k(t)$ vanishes. For condensed-phase systems in which there are many nuclear degrees of freedom and only a few quantum degrees of freedom, the loss of nuclear overlap, *i.e.* the decay of $D_k(t)$, is the dominant mechanism for decoherence.[17] The decoherence function measures the overlap of two initially identical *nuclear* wave functions that propagate in time under the influence of different *electronic* wave functions; it will decay when the electronic wave functions differ in any way. Once the nuclear overlap has decayed, the off-diagonal elements of $\hat{\rho}(t)$ must be zero, forcing the electronic wave function into a mixture of the pure basis states; the classical bath then selects one of the pure states by making a measurement on the quantum subsystem. Therefore, how the nuclear wave function is approximated in a MQC algorithm should determine both how quantum phase information is lost and how different quantum basis states are selected by the bath upon wave function collapse. This provides the definition of decoherence that we will use throughout this paper, and forms the central idea for the development of our new nonadiabatic MQC MD algorithm: decoherence is a bath-induced process that results in total collapse of the quantum wave function to a pure state.

In addition to incorporating decoherence in different ways, MQC MD algorithms are distinguished by how the quantum and classical subsystems are affected by decoherence. The response of the classical subsystem to decoherence is typically designed to conserve the total (quantum + classical) energy, though this is not the only option;[6] the classical response to decoherence is discussed in detail below in Section III.A.2 for our new algorithm and in the Appendix for selected other MQC MD

methods. For the response of the quantum subsystem to decoherence, most nonadiabatic MQC MD algorithms choose which pure state to collapse to stochastically, so the effects of decoherence are modeled as discrete "surface hopping" events between the pure basis states.[2-4] To do this, such algorithms often choose a "reference" state, the last basis state to which the quantum subsystem collapsed, which is treated differently than the other quantum basis states. For algorithms that also use a mean-field (MF) description of the electronic wave function, the use of a reference state leads to two different responses of the quantum subsystem to decoherence. When the TDSE evolves the quantum wave function into a mixture or superposition, surface hopping (*i.e.* nonadiabatic transitions) can occur only to electronic states other than the reference state, and the mixed electronic wave function can be resolved back to the reference state only under special circumstances.[4] Since the choice of a reference state is arbitrary, it is not clear if collapsing preferentially away from (or toward) the reference state provides accurate nonadiabatic quantum dynamics. Moreover, since collapses to and away from the reference state are triggered by different criteria, these MQC MD algorithms are simultaneously employing more than one definition of decoherence. Furthermore, some algorithms also force the quantum subsystem to decohere by adding an exponential decay term to the off-diagonal elements of the electronic density matrix,[7,18,19] or by introducing surface hops that occur over a finite length of time.[7] The time constant for the decay of the off-diagonal density matrix elements or the length of the surface hop introduces yet another criterion for decoherence.

In this paper, we present a new method for performing nonadiabatic MQC MD, which we call "mean-field with stochastic decoherence" (MF-SD), that is based on a unified definition of decoherence: we choose a single collapse criterion that is based on physical arguments and well-defined assumptions about the nuclear wave function in Eqn. 2. We will argue throughout this paper that with this approach, the MF-SD algorithm provides a physically-intuitive mechanism for decoherence that is numerically accurate, computationally efficient, and simple to employ. The rest of this paper is organized as follows. In Section II, we outline the basic procedures for performing MQC MD. In Section III.A, we derive the relevant equations from the nuclear overlap decoherence function, $D_k(t)$ (defined in Eqn. 2), which form the heart of the new MF-SD algorithm. We then present the rest of the equations underlying MF-SD, and in Section III.B we give a point-by-point outline of how to implement the MF-SD algorithm. Section III.C presents a comparison of MF-SD to other nonadiabatic MQC MD algorithms, which are summarized in the Appendix, in terms of how they are implemented, their computational efficiency, and the basic underlying physical principles that each algorithm attempts to capture. In Section IV, we use MF-SD to solve a variety of one-dimensional, two-state scattering problems, and we compare the MF-SD results both to the exact quantum solutions and to the solutions obtained by other MQC methods. Finally, we offer some concluding remarks in Section V. We note that a detailed look at the application of the

MF-SD algorithm to condensed-phase nonadiabatic dynamics, including an exploration of the relaxation dynamics of photoexcited solvated electrons in both water and tetrahydrofuran, will appear in a forthcoming paper.[20] We suggest that readers new to MQC MD algorithms first read Section II, then skip to the Appendix, and finally continue from Section III to the end.

II. Review of Nonadiabatic Mixed Quantum/Classical Molecular Dynamics Methods

We begin our discussion by exploring what makes a MQC MD algorithm desirable and what goes into such an algorithm. First, since MQC algorithms eliminate as many of the quantum coordinates as possible, there must be a prescription to allow the quantum and classical subsystems to interact in a simple and meaningful way. This effective interaction is usually treated via a pseudopotential, $\hat{V}_p(\mathbf{r},\mathbf{R})$, which depends on both the quantal, **r**, and classical, **R**, coordinates. Second, individual trajectories in MQC MD simulations should be physically meaningful – that is, we expect a good algorithm to produce fully coherent TDSE dynamics with classical particles propagated in the presence of the mixed, or mean-field (MF), quantum state, at least over short times.[21] We also expect that a good nonadiabatic MQC algorithm will require the quantum subsystem to resolve occasionally to a pure state due to nuclear-induced decoherence, as suggested by Eqn. 2. Third, the method should be able to model nonadiabatic effects, such as transitions (surface hops) between electronic states. Finally, any good MD algorithm should conserve energy, be computationally efficient, and produce quantitatively accurate quantum observables. In this Section, we discuss features common to all MQC MD algorithms; specific algorithms are differentiated by their treatment of decoherence and nonadiabatic transitions.

Any MQC algorithm starts with the eigenvectors and eigenvalues of the quantum subsystem. Although many alternatives exist, here we will assume the set of adiabatic basis states,[22] defined for each configuration of the classical particles. With this assumption, the properties of the quantum subsystem are given by the time-independent Schrödinger equation

$$\hat{H}(\mathbf{r},\mathbf{R})\left|\phi_j\right\rangle = \varepsilon_j\left|\phi_j\right\rangle, \tag{3}$$

where the Hamiltonian $\hat{H} = \hat{U} + \hat{T} + \hat{V}_p$ has eigenvalues ε_j and adiabatic eigenvectors $|\phi_j\rangle$, $\hat{U}$ and $\hat{T}$ are the quantum potential and kinetic energy operators, and $\hat{V}_p$ is the pseudopotential from the classical particles. The total electronic wave function $|\psi\rangle$ can be written as a superposition of the basis states,

$$\left|\psi\right\rangle = \sum_j c_j\left|\phi_j\right\rangle, \tag{4}$$

where the c_j are time-dependent expansion coefficients and $\sum_j |c_j|^2 = 1$. The dynamics of the quantum subsystem are governed by the TDSE,

$$i\hbar \frac{d|\psi\rangle}{dt} = \hat{H}|\psi\rangle, \tag{5a}$$

which, in turn, governs the evolution of the electronic density matrix elements. By inserting Eqn. 4 into Eqn. 5a and using the electronic density matrix notation of Eqn. 1 with $\rho_{kj} = c_k^* c_j$, the TDSE can be rewritten as,[2]

$$i\hbar \frac{d}{dt}\rho_{kj} = \sum_l \left[\rho_{lj}\left(V_{kl} - \sum_n i\hbar \mathbf{d}_{kl}^n \cdot \dot{\mathbf{R}}_n \right) - \rho_{kl}\left(V_{lj} - \sum_n i\hbar \mathbf{d}_{lj}^n \cdot \dot{\mathbf{R}}_n \right) \right] \tag{5b}$$

where the sum on n runs over the classical nuclear coordinates, $\dot{\mathbf{R}}_n$ is the velocity of nucleus n, and the electronic coupling V_{ij} is given by

$$V_{ij} = \langle \phi_j | \hat{H} | \phi_i \rangle. \tag{6}$$

We note that Eqns. 4 and 5 hold independent of the choice of basis set, but the adiabatic basis provides the advantage of making V_{ij} in Eqn. 6 a diagonal matrix. In the adiabatic basis, $\mathbf{d}_{ij}$ is the nonadiabatic coupling vector, which causes mixing between the basis states and is given by,

$$\mathbf{d}_{ij}^n = \langle \phi_j | \nabla_{\mathbf{R}_n} \phi_i \rangle, \tag{7}$$

where $\nabla_{\mathbf{R}_n}$ is the gradient with respect to the classical coordinate, $\mathbf{R}$, associated with nucleus n. In order to conserve the total energy of the mixed quantum/classical system, the effect of the mixed, or mean field wave function $|\psi(t)\rangle$ on the classical particles is given by the Hellyman-Feynman (HF) expression,

$$\mathbf{F}^n(t) = -\nabla_{\mathbf{R}_n} \langle \psi(t)|\hat{H}|\psi(t)\rangle = \langle \psi(t)| - \nabla_{\mathbf{R}_n} \hat{V}_p |\psi(t)\rangle, \tag{8}$$

where $\mathbf{F}^n(t)$ is the force of the quantum subsystem on nucleus n at time t, and the last equality in Eqn. 8 holds because the classical gradient does not affect either the quantum kinetic or potential energy operators. The HF force provides feedback about the quantum dynamics to the classical particles, allowing the subsystems to interact. The sum of the classical forces and the HF force is then used by a classical MD algorithm to determine new classical particle positions at the end of each simulation step, and these new positions determine the eigenvalues and eigenvectors of the quantum subsystem through Eqn. 3. The most general formulation of a coherent mixed quantum/classical MD simulation using the adiabatic basis set is simply the repeated execution of the above statements.

Finally, we note that the above expressions also can be used to perform fully adiabatic dynamics. All that is required is to set the expansion coefficients c_i in Eqn. 4 to zero for all i except the state of interest, to set all of the nonadiabatic coupling vectors, $\mathbf{d}_{ij}$, in Eqn. 5b to zero, and to reduce Eqn. 8 to the adiabatic HF force,

$$\mathbf{F}_i^n(t) = \langle \phi_i | - \nabla_{\mathbf{R}_n} \hat{V}_p | \phi_i \rangle. \tag{9}$$

If, however, Eqns. 5-8 are used for nonadiabatic dynamics, then the algorithm that implements them must also include a method for implementing nonadiabatic transitions and decoherence. We have summarized the salient features of several nonadiabatic MQC MD methods in the Appendix and Table I, and readers new to the field of MQC MD are urged to read the Appendix before moving on to Section III; further information about many nonadiabatic MQC MD algorithms is provided in an excellent review article by Drukker.[23]

III. Mean Field Dynamics with Stochastic Decoherence (MF-SD)

In this section, we derive a new algorithm, called mean field with stochastic decoherence (MF-SD), which we believe contains a physically motivated and accurate description of decoherence and combines the best features of the methods discussed in the Appendix with minimal disadvantages and only a single *ad hoc* parameter; we will show below that although we have not been able to derive a rigorous expression for this parameter, we have found that its value is in fact defined by the system being simulated and is not free.

A. The Ideas Underlying MF-SD

We start our development of MF-SD using the set of adiabatic basis states and choosing the TDSE to govern the dynamics of the MQC trajectories, resulting in a MF description for propagation of the electronic degrees of freedom in the presence of the classical particles; in this way, each MF-SD trajectory is physically meaningful. As we will discuss further below, decoherence of the electronic density matrix is modeled in MF-SD simulations as an instantaneous, total collapse of the MF wave function to one of the adiabatic basis states. We choose to collapse to adiabatic states in MF-SD because they are the eigenvectors that define the quantum subsystem for frozen configurations of the solvent, and since we take decoherence events in MF-SD to be instantaneous, the classical subsystem is frozen during these events. Thus, MF-SD assumes that decoherence is not basis independent, a result that might be expected on physical grounds. One difference between MF-SD and other nonadiabatic MQC MD methods is that MF-SD is based on a single criterion for instantaneous wave function collapse, no matter which pure state is selected. This is an advantage because MF-SD does not require a "reference" state,[2,4,5] multiple definitions of decoherence,[4,7,18] or multiple simultaneous trajectories for each classical initial condition.[2,4,5,18,19] We will show below that this choice also allows MF-SD to improve upon other MQC MD methods in terms of computational efficiency and, in most cases, accuracy.

1. Deriving a Decoherence Time for MF-SD: In this subsection, we derive an expression that determines the rate at which the classical particles induce decoherence, and present a prescription for the response of the quantum subsystem when a decoherence event takes place. For MF-SD, we wish to

choose a criterion based on the decoherence function, $D_k(t)$, defined in Eqn. 2, which can be rewritten as

$$D_k(t) = \left\langle \chi_k(t) \middle| \chi(t) \right\rangle = \left\langle \chi(0) \middle| e^{i\hat{H}_k t/\hbar} e^{-i\hat{H}t/\hbar} \middle| \chi(0) \right\rangle, \tag{10a}$$

where $\hat{H}$ is the Hamiltonian that evolves the full superposition electronic wave function and $\hat{H}_k$ is associated with propagation on the k^{th} adiabatic electronic surface. Equation 10a is similar to an expression studied by Neria and Nitzan that involves the overlap of nuclear wave packets propagated under the influence of two different adiabatic states,[24]

$$D_{k,k'}(t) = \left\langle \chi(0) \middle| e^{i\hat{H}_k t/\hbar} e^{-i\hat{H}_{k'} t/\hbar} \middle| \chi(0) \right\rangle. \tag{10b}$$

The important distinction is that $D_k(t)$ (Eqn. 10a) measures the decay of nuclear overlap caused by propagation between an adiabatic state and the full superposition state, whereas $D_{k,k'}(t)$ (Eqn. 10b) measures the decay caused by propagation on two pure adiabatic states. Eqns. 10a and 10b describe a process that begins with two identical (in initial position, width, and momentum) nuclear wave packets, each of which begins a trajectory on a different electronic state. Since the electronic surfaces are distinct, as time passes, the nuclear wave packets will eventually lose spatial and momentum overlap. For the case of propagation on two different adiabatic states, Schwartz *et al.* used the frozen Gaussian approximation[25] for the nuclear wave function and expanded Eqn. 10b at short times to calculate the decay of the nuclear overlap.[26] If we use the same approach[26] and approximations[27] in Eqn. 10a, then $D_k(t)$ can be rewritten,

$$D_k(t) \approx \exp\left[-\sum_n \frac{\left(\mathbf{F}^n(0) - \mathbf{F}_k^n(0) \right)^2}{4 a_n \hbar^2} t^2 \right] \tag{11}$$

where for each classical nucleus n at time zero, $\mathbf{F}_k^n(0)$ is the adiabatic HF force from state k (Eqn. 9), $\mathbf{F}^n(0)$ is the full mean field HF force (Eqn. 8), and a_n is the inverse of the square of the width of the n^{th} frozen Gaussian wave packet. Since $D_k(t)$ determines the decay of the off-diagonal elements of the total density matrix (Eqn. 2), we can use Eqn. 11 to define the *decoherence time*,

$$\tau_k^{-2} = \sum_n \frac{\left(\mathbf{F}^n(0) - \mathbf{F}_k^n(0) \right)^2}{4 a_n \hbar^2}. \tag{12}$$

where τ_k is the characteristic time constant of the Gaussian decay of $D_k(t)$ that results from the fact that the nuclear degrees of freedom diverge when propagated under the influence of adiabatic state $|\phi_k\rangle$ instead of the full superposition state $|\psi\rangle$. Equation 12 defines a unique decoherence time for each adiabatic state at every classical configuration; this time depends on only a single parameter, a_n, which depends on the width of the frozen Gaussian chosen to represent nucleus n. In other applications of the frozen Gaussian approximation, a_n is defined by the *thermal* deBroglie wavelength of classical nucleus n,[24] but we will argue in Section IV.D that for MF-SD this parameter is related to the spatial extent of the nonadiabatic coupling and the *instantaneous* deBroglie wavelength. In our view of decoherence, when the nuclear

overlap has decayed, the quantum subsystem must collapse onto one of the adiabatic states; thus, we will use τ_k to govern the total collapse of the quantum subsystem and not just the decay of the off-diagonal elements of the electronic density matrix. We choose $1/\tau_k$ to serve as the operative MF-SD definition of the rate for nuclear-induced wave function collapse (decoherence) to adiabatic eigenstate k. With this choice, MF-SD does not distinguish between decoherence and what others refer to as "nonadiabatic transitions": the mean-field wave function can collapse to any of the adiabatic states with the rates given by Eqn. 12.

To determine precisely when a collapse should occur in MF-SD, we define the probability, P_k, for the mean-field wave function to collapse to the k^{th} adiabatic eigenstate as

$$P_k = \frac{\rho_{kk}}{\tau_k} dt \,, \tag{13}$$

where we have multiplied the inverse of the decoherence time by the simulation time step, dt, and weighted the probability by the population on state k, ρ_{kk}. The weighting by ρ_{kk} makes the probability for collapse proportional to the population of each adiabatic state in the full mixed wave function, as is usually assumed in theories of quantum measurement; in this way, the system is prevented from collapsing to adiabatic eigenstates that have no amplitude. In the limit that there is no decoherence, this choice recovers the exact TDSE probabilities for fully coherent propagation. In the MF-SD algorithm, we implement decoherence stochastically by comparing the probability computed from Eqn. 13 to a random number, ξ, chosen uniformly on [0,1), and we force the wave function to collapse to adiabatic state k whenever $P_k > \xi$. When we force a collapse, we set all the elements (diagonal and off-diagonal) in the electronic density matrix to zero, except $\rho_{kk} = 1$.[28]

In the event that collapses to more than one adiabatic state are allowed (when ξ is less than two or more of the P_k's), which is a potential issue with any stochastic surface hopping algorithm,[2,4,7] we recast the probabilities relative to the set of allowed collapses by

$$T_j = P'_j + C_{j-1}, \tag{14}$$

where

$$P'_j = \begin{cases} P_j / P_{sum} & j \in \text{allowed} \\ 0 & j \notin \text{allowed} \end{cases}, \tag{15}$$

with

$$P_{sum} = \sum_{j \in allowed} P_j \tag{16}$$

and

$$C_j = \sum_{i=1}^{j} P_i' . \tag{17}$$

This ensures that the new set of probabilities, T_j, run from [0,1]. We then choose a new random number on [0,1), ξ', and require the quantum subsystem to collapse to state k whenever

$$T_{k-1} < \xi' < T_k . \tag{18}$$

With these choices, collapses of the wave function in MF-SD occur to each adiabatic state in a manner proportional both to the population of that state in the full mixed wave function and to how effective that state is in leading to the loss of nuclear overlap.

We finish this subsection by examining the decoherence time in more detail. Equation 12 says that decreasing the nuclear frozen Gaussian width (i.e. making a_n larger) causes the nuclear overlap to decay more slowly and thereby increases the decoherence time, which at first seems counterintuitive. However, in the short-time expansion of Eqn. 10a that leads to Eqn. 12, the position part of the frozen Gaussian wave packet overlap cancels to second order in time and the force difference that remains arises from the momentum part of the frozen Gaussians.[26] Since the nuclear width in position space is inversely proportional to the momentum uncertainty, the wider the Gaussian wave packet is in position space, the more quickly the overlap between nuclear wavepackets is lost. Thus, the decoherence rate we choose for MF-SD, Eqn. 12, is actually a momentum-based criterion.

2. Conservation of Energy and "Forbidden" Transitions in MF-SD: Now that we have introduced a new method for the classical particles to induce collapses of the quantum wave function, we turn in this subsection to the details of how the classical subsystem responds to a decoherence event. When the mixed wave function collapses to state k, the quantum energy changes discontinuously from $E_{MF} = \langle \psi | \hat{H} | \psi \rangle$ to the adiabatic eigenvalue, ε_k. To conserve the total (quantum + classical) energy of the system in MF-SD, we scale the classical kinetic energy in a manner similar to other MQC MD methods[2,4] to compensate for the change in quantum energy. After a decoherence event in MF-SD, the classical velocities, $\mathbf{v}_n(t)$, become

$$\mathbf{v}_n'(t) = \mathbf{v}_n(t) - \gamma \mathbf{d}_k^n(t) . \tag{19}$$

where instead of scaling the classical velocities along the direction of the nonadiabatic coupling vector (Eqn. 7) as is done in other algorithms, we scale the classical velocities in the direction of an *effective* mean-field nonadiabatic coupling vector,

$$\mathbf{d}_k^n = \sum_{i \neq k} \rho_{ii} \left\langle \phi_k \left| \nabla_{\mathbf{R}_n} \phi_i \right. \right\rangle = \sum_{i \neq k} \rho_{ii} \mathbf{d}_{ik}^n , \tag{20}$$

which is the MF population-weighted average of the $\mathbf{d}_{ik}^n$ defined in Eqn. 7.[5] The scalar γ in Eqn. 19 is

determined by solving a quadratic equation based on the constraint that the change in classical kinetic energy (KE) must be equal and opposite in magnitude to the change in the quantum energy (QE):[29]

$$\Delta KE = KE_{new} - KE_{old} = -\Delta QE = QE_{old} - QE_{new}$$
$$KE_{new} = \frac{1}{2}\sum_n m_n \left(\mathbf{v}'_n\right)^2; \qquad KE_{old} = \frac{1}{2}\sum_n m_n \left(\mathbf{v}_n\right)^2 \tag{21}$$
$$\frac{\gamma^2}{2}\sum_n m_n \left(\mathbf{d}_j^n\right)^2 - \gamma \sum_n m_n \left(\mathbf{v}_n \cdot \mathbf{d}_j^n\right) + \Delta QE = 0$$

where $\Delta KE = -\Delta QE$ is the difference between the classical kinetic energy before (old) and after (new) the decoherence event and m_n is the mass of nucleus n. We choose to rescale the classical velocities along the effective MF non-adiabatic coupling vector (Eqn. 20) because only those classical motions with components along this vector cause the adiabatic states to mix, so only these degrees of freedom should contribute to the discontinuity in quantum energy.

Some collapses (decoherence events) lead to an increase in the energy of the quantum subsystem, so it is possible for the classical subsystem to have insufficient kinetic energy along the effective nonadiabatic coupling vector to give to the quantum subsystem. This means that the total energy cannot be conserved for this event, and the upward quantum transition is considered "forbidden". Most MQC MD methods assume that such forbidden transitions correspond to classical turning points,[29] and in these instances, the classical momentum is typically reversed along the direction of the nonadiabatic coupling vector, leaving the quantum subsystem unchanged. We note, however, that Müller and Stock have argued that simply ignoring forbidden transitions and not reversing the classical velocities leads to an improvement in the accuracy of the calculated quantum branching ratios.[30] As such, for MF-SD, we choose to ignore all forbidden transitions.

The issue of forbidden upward transitions also produces the following conundrum. Suppose for a particular configuration that both an upward transition, to state k^+, and a downward transition, to state k^-, are allowed based on the random number ξ and the probabilities in Eqn. 13. In MF-SD, we recast the transition probabilities according to Eqns. 14–17. If the upward transition is chosen by the *second* random number, ξ' (see Eqn. 18), then the system should collapse to state k^+. If there is insufficient classical kinetic energy along the direction of the effective nonadiabatic coupling vector (i.e. there is no γ that satisfies Eqn. 21 and the conditions outlined above), then the collapse to state k^+ is forbidden. The original random number, however, indicated that either transition was likely, and the downward collapse to state k^- is always allowed by energy conservation. So the question in this case is whether the quantum system should remain in the fully mixed state or should collapse to state k^-. Accepting the collapse to state k^- would amount to a modification of the probabilities in Eqn. 13 such that

$$P_j = \left[\frac{\rho_{jj}}{\tau_j} dt \right] \Theta(KE_{cl}) \tag{22}$$

where

$$\Theta(KE_{cl}) = \begin{cases} 1 & \text{Energy allowed} \\ 0 & \text{Energy forbidden} \end{cases} \tag{23}$$

is a step-function that depends on the available classical kinetic energy (KE_{cl}) along the effective MF nonadiabtic coupling vector. We implemented MF-SD using decoherence probabilities described by both Eqns. 13 and 22 for the one-dimensional, single avoided crossing example that will be discussed below in Section IV A, and found that inclusion of the energy-dependent step-function incorrectly predicted no reflection on the lower surface at $k \sim 8$ a.u. (*cf.* Fig. 2c, below). Thus, all the other MF-SD simulations discussed in this paper use the decoherence probabilities defined by Eqn. 13, not the energy-dependent probabilities in Eqn. 22. In fact, any nonadiabatic MQC algorithm that includes instantaneous changes to the quantum wave function[2,4,5,18,19] should suffer from this same conundrum, but to the best our knowledge, the issue of how to resolve it has not been previously addressed in the literature.

B. Point-by-Point Outline of the MF-SD Algorithm

In this section, we present a point-by-point outline of each step required to implement the MF-SD algorithm. The user is required to find a way to integrate the time-dependent Schrödinger equation, a simple and efficient way to generate the MQC Hamiltonian, and a way to find the adiabatic eigenvectors and eigenvalues. The initial trajectory setup requires a position and momentum to be assigned to each classical particle, an initial seed for the random number generator, and an initial electronic density matrix, which may represent a pure state, a mixture, or a superposition of states. Once the initialization is complete, the implementation of MF-SD proceeds as follows:

1. For the configuration of the classical coordinates at time t, $\mathbf{R}(t)$, find the adiabatic basis states (the eigenvalues and eigenvectors of the Hamiltonian) using Eqn. 3.

2. Using Eqn. 5b, integrate the TDSE to the current time, t, to find the density matrix elements and the mean-field wave function (Eqn. 2).

3. Calculate the mean-field HF force on each nucleus, $\mathbf{F}^n(t)$ and the HF force from each of the adiabatic states, $\mathbf{F}^n_j(t)$ using Eqns. 8 and 9, respectively.

4. Using the forces obtained in Step 3 and the choice for a_n given below in Eqn. 24, calculate the decoherence probabilities for each of the adiabatic states, P_k, using Eqn. 13. Once the P_k's are obtained, determine whether or not the system has collapsed by calling a random number, ξ, from [0,1).

4.1. If a single $P_k > \xi$, then collapse the MF wave function to the adiabatic state ϕ_k using the procedure described in Step 5.

4.2. If more than one $P_k > \xi$, then perform the "tie-breaker" test using Eqns. 14-18 to choose the appropriate adiabatic state for the collapse, and proceed to Step 5.

4.3. If all of the $P_k < \xi$, then no collapse occurs; skip to Step 6.

5. If the tests in Step 4 determine that a collapse should occur,

5.1. Calculate the effective nonadiabatic coupling vector using Eqn. 20.

5.2. Solve Eqn. 21 for γ; if the collapse is allowed, proceed to 5.3; if the collapse requires an energetically upward hop for the quantum subsystem and no solution for γ exists (i.e. conservation of energy is not satisfied), do not perform the wave function collapse, do not set ψ to ϕ_k, do not rescale the classical velocities; instead, skip to Step 6.

5.3. (a) set the mean-field HF force to the adiabatic force for state k chosen in Step 4, i.e. $\mathbf{F}(t) = \mathbf{F}_k(t)$; (b) reset the electronic density matrix to represent the pure state, k (i.e. set all elements of the matrix to zero except $\rho_{kk} = 1$), and (c) and rescale the classical velocities using γ from Eqn. 21.

6. Calculate the classical forces, $\mathbf{f}(t)$.

7. Propagate the classical equations of motion using the quantum and classical forces, $\mathbf{F}(t)$ and $\mathbf{f}(t)$, to generate a new classical configuration, $\mathbf{R}(t+dt)$ with any classical MD algorithm, and return to Step 1.

C. Comparison of the Ideas in MF-SD to Other MQC MD Algorithms: In this subsection, we compare and contrast MF-SD to some other MQC MD methods, whose features are discussed in more detail in the Appendix. We first turn to the issue of computational expense; ignoring the cost of the features common to all MQC MD algorithms (see Section II), it is clear that different methods of treating decoherence do in fact change the cost of an algorithm. For example, in the mean-field with surface hopping (MFSH) algorithm of Prezhdo and Rossky[4] (see Appendix Section C), decoherence events are determined by comparing the dynamics of a MF trajectory to those of a second, simultaneous adiabatic MQC trajectory. The fact that two trajectories with different solutions to the Schrödinger equation must be used to determine the MFSH dynamics makes MFSH roughly twice as computationally expensive as MF-SD. In the fewest-switches surface hopping (FSSH) algorithm of Tully[2] (also sometimes referred to in the literature as molecular dynamics with electronic transitions, or MDET; see Appendix Section A), the individual trajectories are fully adiabatic with discrete hops between adiabatic states, and decoherence takes place by adding together a swarm of trajectories for each classical initial condition at the amplitude level. Thus, the dynamics of individual FSSH trajectories are not physical, and it is unclear how many trajectories in the swarm must be averaged before observables can be calculated. The need for a

trajectory swarm of unknown size can make FSSH significantly more expensive than MF-SD. MF-SD is also more efficient than the stationary phase surface hopping (SPSH) algorithm of Webster *et al*. (see Appendix Section B),[3] which requires an iterative evaluation of the quantum forces using the Pechukas method[31] to propagate the classical degrees of freedom. Finally, MF-SD is much more efficient than Martinez's[6] full-multiple spawning method (FMS, see Appendix Section D), since the number of spawned basis functions (each of which are essentially separate semiclassical trajectories) may be dozens or hundreds for each classical starting configuration. In MF-SD, the only computational expense not shared by other MQC MD algorithms is the calculation of the decoherence times, Eqn. 12, but for a moderate number of basis states in the condensed phase,[20] this calculation is no slower than diagonalization of the Hamiltonian. Overall, MF-SD provides for evolution of the quantum subsystem via the TDSE with decoherence events that do not require a swarm of trajectories, so each individual MF-SD trajectory contains physically meaningful quantum dynamics.

Of course, the most important feature of any MQC MD algorithm is its accuracy: even if an algorithm is efficient and easy to implement, it is of little utility if it does not provide accurate results. As we will explore in detail below in Section IV, MF-SD is indeed quantitatively accurate, and on some problems it performs better than other MQC MD methods. We believe this is because MF-SD incorporates a more physical definition of decoherence.

In summary, even though decoherence cannot be formally derived from the TDSE, the way decoherence is implemented in the MF-SD algorithm is grounded in specific assumptions regarding the total quantum/classical density matrix and the nuclear wave function.[32] In contrast, fully adiabatic methods such as FSSH do not address decoherence in individual trajectories, and most mean field methods use *ad hoc* criteria and/or many different definitions of decoherence that are not based on well-defined assumptions about quantum nature of the bath. We note that a recent paper by Jasper and Truhlar[33] derived a decoherence time by making different assumptions about the nuclear wave function and taking the first time-derivative of $D_{k,k'}(t)$ in Eqn. 10b. Their derivation led to a decoherence time that depends on both the spatial and momentum overlap of the nuclear wavepackets, whereas our decoherence formula, Eqn. 12, contains only a momentum criterion. Although MF-SD is fully compatible with *any* nuclear-induced decoherence time inserted into Eqn. 13, the decoherence time derived by Jasper and Truhlar is more difficult to calculate than Eqn. 12.[33]

IV. Application of MF-SD to Two-State Nonadiabatic Model Systems

In the MF-SD algorithm, decoherence is accounted for by making the frozen Gaussian approximation for the nuclear wave function and assuming that the decay of nuclear overlap, $D_k(t)$, causes the electronic wave function to lose coherence; MF-SD uses this decay to calculate the decoherence rate.

The quantum subsystem responds to the nuclear-induced decoherence by collapsing to a pure state so that all quantum coherence is destroyed. The collapse may or may not leave the system on a different electronic surface than the one it started on, providing a means to account for what other nonadiabatic MQC methods call "nonadiabatic transitions". In this section, we use simple, one-dimensional (1-D) model problems to determine whether the new MF-SD algorithm provides sufficient accuracy for quantum dynamics in the absence of the Born-Oppenheimer approximation. The model nonadiabatic systems we discuss here were presented in Ref. 2, and include: a single avoided crossing; a dual avoided crossing; and a system with an extended range of nonadiabatic coupling. For each of these three model problems, we show the adiabatic surfaces in Figure 1 and the results of both exact and MQC MD calculations in Figures 2, 3, and 5.

To apply MF-SD to the three test problems, we begin by following Ref. 2 and choosing the mass of the classical particle to be 2000 a.u. We performed the classical integration using the velocity Verlet algorithm, and the integration of the quantum density matrix with a fourth-order Runge-Kutta algorithm with 150 intermediate points to propagate the electronic density matrix over the duration of a single classical time step. Each trajectory began with the classical particle on the lower adiabatic quantum surface at $x = -10$ a.u. The particle was given incident momentum to the right and the simulations were run until the classical particle reached a position of $|x| = 15$ a.u. Fewer than 0.5% of all trajectories failed to leave the interaction region after 2.5×10^5 classical time steps, and these were not included in the averaging. The simulation time step was chosen so that the fluctuation in the total (quantum + classical) energy for any single trajectory was less than 3%, though this error is easily reduced with shorter time steps. All of the calculations performed here used the RAN3 random number generator.[34] The MF-SD simulations all used the adiabatic basis, and the results we present in Figures 2, 3 and 5 are averages of the final values of ρ_{11} and ρ_{22} over 2000 trajectories per initial momentum.

We note, however, that trajectories with a low enough initial momentum never have sufficient energy to fully occupy the upper adiabatic state. As the single avoided crossing problem shows in Figure 1a, in order to conserve the total energy, the classical particle must have at least 0.02 Hartree of kinetic energy, $k > \sim 5$ a.u., at the beginning of the trajectory to be observed in the upper state to the far right or left at the end of the trajectory. To conserve energy for the dual avoided crossing, the initial momentum must be $k > \sim 14$ a.u. ($log(E/\text{a.u.}) > -3$), and the classical particle in the extended coupling model must have initial momentum $k > \sim 29$ a.u. for transmission on the upper surface.[35] In these cases of low initial momentum, no energy-conserving decoherence event ("measurement") could cause the system to be observed in the upper state. As such, at the end of trajectories that had insufficient initial energy to occupy the upper adiabatic surface, we forced the final mixed state to collapse to the lower surface. This is justified because the adiabatic surfaces still have an infinitesimally small slope, meaning that a

decoherence event that collapses the system to the lower surface would eventually occur for a sufficiently long trajectory because upward transitions would have been forbidden. In contrast, the FSSH and MFSH algorithms calculate the upper/lower state branching ratio by counting the last reference state, regardless of the amount of mixing at the end of the trajectory; for MFSH, this amounts to performing a mean-field rescaling (see Appendix Section C) at the end of each individual trajectory, regardless of the available energy.

The only parameter in the MF-SD algorithm is the width of the frozen Gaussian wave packet representing each classical nucleus. Other applications with frozen Gaussians have taken a_n to be given by the thermal deBroglie wavelength, however, we believe that a microscopic algorithm should rely only on instantaneous rather than thermally-averaged information about the classical particles. For reasons that we discuss below in Section IV.D, we chose this width to be

$$a_n(t) = \left(\frac{(w/a_0)^2}{2\lambda_D(t)} \right)^2 \tag{24}$$

where $\lambda_D = h/mv$ is the instantaneous deBroglie wavelength of the classical particle, a_0 is the Bohr radius, v is the classical velocity at time t, and w is the spatial extent of the nonadiabatic coupling, discussed in Section IV.D. For the 1-D problems explored here, the coupling width, w, was chosen to be approximately the width of the Gaussian (or exponential), $V_{12}(x)$, in the diabatic coupling matrix.

A. Single-Avoided Crossing

The diabatic Hamiltonian for the single-avoided crossing model is:[2]

$$\begin{aligned} V_{11}(x) &= A[1 - \exp(-Bx)] \qquad x > 0 \\ V_{11}(x) &= -A[1 - \exp(-Bx)] \qquad x < 0 \\ V_{22}(x) &= -V_{11}(x) \\ V_{12}(x) &= V_{21}(x) = C\exp(-Dx^2) \end{aligned} \tag{25}$$

where $A = 0.01$, $B = 1.6$, $C = 0.005$, and $D = 1.0$, all in atomic units, with the coupling width $w = 1/\sqrt{D} = 1\ a_0$. The MF-SD solutions to this problem as a function of incident particle momentum, k, are presented as the boxes connected by solid lines in Figure 2, which show the probability for the classical particle to be transmitted on the lower state (Fig. 2a), transmitted on the upper state (Fig. 2b), or reflected back to the left on the lower state (Fig. 2c). For comparison, we also show the results from FSSH calculations (grey triangles) and the exact quantum mechanical solutions (grey open circles), both calculated by Tully.[2,36] The MF-SD calculations for transmission do not quantitatively agree with either the exact or FSSH results at intermediate momenta, $6 < k < 15$, but MF-SD is more accurate at higher momentum ($k > 20$) than FSSH. Both MF-SD and FSSH methods fail to obtain tunneling of the classical particle through the

barrier on the lower surface at very low momentum, which is represented by the step-function behavior below k = 5 a.u.; this is a well-known failing of almost all MQC MD methods, FMS excepted.[6] Both MF-SD and FSSH also accurately calculate the small amount of particle reflection that occurs when k = ~8 a.u. (Fig 1c), which is above the threshold for transmission. This reflection is accounted for by trajectories that have upward quantum transitions, get trapped in the well on the excited state, and then make a downward transition while travelling to the left.

B. Dual-Avoided Crossing

The key feature of the dual avoided crossing model is quantum-interference effects (Stueckelberg oscillations)[2] that come from the successive regions of strong nonadiabatic coupling. The model diabatic potential is given by[2]

$$\begin{aligned} V_{11}(x) &= 0 \\ V_{22}(x) &= -A\exp(-Bx^2) + E \\ V_{12}(x) &= V_{21}(x) = C\exp(-Dx^2) \end{aligned} \tag{26}$$

where A = 0.10, B = 0.28, C = 0.015, D = 0.06, and E = 0.05, all in atomic units; the coupling width is $w = 4\ a_0 \approx 1/\sqrt{D}$. The exact results (solid grey circles) in Fig. 3 were taken from Ref. 4.[36] The MF-SD (boxes connected by solid lines), FSSH (triangles),[2] and MFSH (exes)[4] results are all in qualitative agreement for the transmission probabilities, exhibiting the expected oscillations for transmission on the upper and lower surfaces. The SPSH results (not shown; see Fig. 1 of Ref. 3b), are also qualitatively correct,[3b] and the full multiple spawning (FMS) results (not shown; see Fig. 7 of Ref. 6c) are in quantitative agreement as well.[6] The magnitude of the oscillations is good for all of the approximate methods, but at low energy, the phase of the oscillations calculated by all of the MQC methods is mis-matched from the exact result, although MFSH comes closest. It is not surprising that all of the approximate methods are in agreement with the exact oscillations at high energy. Since there is rigorously no reflection above $log_e(E/\text{a.u.}) > \sim -3$, the oscillations in the transmission probabilities merely reflect the density matrix elements associated with the upper or lower surfaces; any method that integrates the TDSE properly should obtain the correct results at these energies.

Although all of the MQC MD methods accurately calculate the transmission probabilities for this problem, MFSH and FSSH fail to accurately calculate the reflection probabilities by an order of magnitude, as shown in Fig. 3c (note the expanded scale); reflection results for SPSH were not given in Ref. 3. MF-SD, however, obtains the correct transmission/reflection branching ratio. This overestimation by FSSH and MFSH arises because the transition probability from the FSSH algorithm (on which MFSH is also based) results in too many upward transitions. To better understand this overestimation, in Figure 4 we plot transition probabilities for MF-SD and FSSH for an adiabatic ground

state trajectory as a function of position for a classical particle initially with k = 14.14 a.u. or $log_e(E/\text{a.u.})$ = –3; the adiabatic surfaces (dashed grey curves) are shown to guide the eye. The *minimum* probability for a nonadiabatic transition in the FSSH algorithm (dotted curve) is

$$P_{FSSH}^{\min} = 2(\mathbf{v} \bullet \mathbf{d}_{12})dt \tag{27a}$$

(see Eqns. A1 and A2) where dt = 0.3 a.u. is the simulation time-step.[37] The reason that $P_{FSSH}^{\min}$ is a minimum is because in the implementation of FSSH, Eqn. 27a is divided by a fraction (in this case, the diagonal element of the fictitious density matrix corresponding to the reference state). Figure 4 also plots the *maximum* decoherence probability from the MF-SD algorithm (solid curve), which is given by

$$P_{MF-SD}^{\max} = \frac{dt}{\tau_2} \tag{27b}$$

(see Eqn. 13). $P_{MF-SD}^{\max}$ is a maximum for two reasons: First, in the implementation of MF-SD, Eqn. 27b is multiplied by a fraction (the population on state 2) and second, the force difference used to calculate τ_2 in Eqn. 27b is the *adiabatic* force difference between states 1 and 2 (*cf*. Eqn. 9). Thus, Figure 4 suggests that in the dual avoided crossing problem, the probability for a nonadiabatic transition to the upper surface in FSSH is *more than* 20 times greater than the corresponding probability in MF-SD.

We can safely assume at these low energies that once a trajectory makes an upward transition, it has a roughly equal chance of being transmitted or reflected on the lower surface in FSSH or MF-SD. Therefore, if >20 times more FSSH trajectories make the upward transition than MF-SD trajectories, we should expect to see >20 times more reflection probability. However, Fig. 3c shows that FSSH overestimates the probability for reflection by only a factor of 10, not 20 or more. The reason for this is that with FSSH, each trajectory can only make a transition when the position of the classical particle is on the left (x < 0),[37] whereas MF-SD trajectories can make transitions over the entire range of the well, effectively doubling the number of chances MF-SD simulations have for collapsing to the upper state. As a result, FSSH (and MFSH, which uses the FSSH transition probabilities) overestimate the amount of reflection by roughly a factor of 10. MF-SD, using a physically motivated and unified definition of decoherence, correctly captures the physics of this reflection.

C. Extended Coupling

The diabatic potential for the extended coupling model problem is[1]

$$\begin{aligned} V_{11}(x) &= A \\ V_{22}(x) &= -A \\ V_{12}(x) = V_{21}(x) &= C\exp(-Dx) \qquad x < 0 \\ V_{12}(x) = V_{21}(x) &= C\left[2 - \exp(-Dx)\right] \qquad x > 0 \end{aligned} \tag{28}$$

where $A = 6\text{x}10^{-4}$, $C = 0.1$ and $D = 0.9$, all in atomic units; we chose $w = 1\ a_0 \approx 1/D$. As the results of Figure 5 indicate, the extended-coupling model is a particularly difficult system for the MFSH and FSSH algorithms; MFSH[4] (exes connected by lines) and FSSH (not shown; see Fig. 6 in Ref. 2) both predict large, rapid oscillations in the reflection coefficients that are not present in the exact QM result (grey circles).[38] The MF-SD (solid curve with boxes) and FMS (not shown; see Fig. 8 from Ref. 6c) algorithms, however, do not exhibit the oscillations that plague the other two MQC MD methods. Of course, the extended coupling system should not show any Stueckelberg oscillations because as the nuclear wave function leaves the coupling region and enters the region where the adiabatic states split, part of the wave function will be reflected on the upper surface, and part will be transmitted on the lower surface. The reflected and transmitted parts of the wave function do not encounter each other ever again and therefore cannot interfere. The artificial oscillations in FSSH and MFSH result from trajectories that get reflected by the upper surface, and as they re-enter the region of strong nonadiabatic coupling, the quantum subsystem freely hops (changing the "reference" state) between the upper and lower surfaces as the particle exists to the far left. Thus, the oscillations most likely occur because the amount of time spent in the strong coupling region varies with the particle's momentum. In contrast, MF-SD has no reference state; thus, once the system is reflected, the mean-field force and the force from each of the adiabatic states become similar, so decoherence events occur only rarely (effectively only once as $t \rightarrow \infty$). This is an important distinction between MF-SD and other MQC MD methods that use the FSSH criteria.[2,4,5,18,19] The FSSH algorithm calls for surface hops when the nonadiabatic coupling is highest; in this case, when the classical particle has a position approximately $-7 < x < -3$. The fact that the FSSH probability (Eqn. A.1) is largest when the classical and quantum subsystems are not interacting (the Hellmann-Feynman force is nearly zero in this range) leads to trajectories that do not properly incorporate decoherence; thus FSSH-based methods cannot obtain the correct reflection probabilities.[39] In MF-SD, however, decoherence occurs when the force difference is largest, just to the right of $x = 0$ at the inflection point of the two adiabatic surfaces and where the quantum and classical subsystems are affecting each other the most strongly. Moreover, when the classical and quantum subsystems no longer interact because the quantum subsystem does not exert any force on the classical particle, as is the case for $|x| > \sim 4$, there should be no decoherence. MF-SD predicts this correctly because the mean-field HF forces and the adiabatic forces are all zero; thus, MF-SD trajectories can be completed with the quantum subsystem still in a superposition state, as the exact results show should be the case for this particular model problem.

D. Exploring the Interaction Width w *and the Nuclear Gaussian Width* a_n

In this section, we discuss the system-defined parameter in the MF-SD algorithm, called the interaction width w, which is used to set the widths of the frozen Gaussians centered on each classical

nucleus. The origin of Eqn. 24 is empirical, but we found that this relationship was necessary to obtain the best results for the three problems presented in Figures 2, 3, and 5. There are two ways we can test the validity of our expression for w: we can either change the width of the coupling in the model potential and use the new width to define a new frozen Gaussian wavepacket, or we can change the width of the Gaussian wavepacket for a fixed coupling width. The dual-avoided crossing is a good model problem for these tests because it is the only one of the three model potentials with $w \neq 1$ and because the Stueckelberg oscillations are sensitive both to the separation between the two regions of coupling and to the ability of the particle to interact with the two crossings simultaneously. For example, Webster *et. al.*[3b] observed that as the separation between the two regions of strong nonadiabatic coupling is increased, a fully quantum wave packet will only interact with one crossing at a time. Conversely, as the coupling is narrowed, the system resembles a single crossing event. In this section, we first change the system, apply the empirical relationship for the system-defined interaction width, and show that with this choice, MF-SD still calculates the correct quantum observables. Then, for a single system, we show that small changes to w have little effect on the calculations, but that larger changes in w result in wildly inaccurate branching ratios.

Figure 6 shows the survival probability for a particle *initially on the upper surface* for a narrow dual avoided crossing (Eqn. 26) in an attempt to verify the emperical relationship between w and the nonadiabatic coupling width. The only difference between the adiabatic surfaces shown in Figure 1b and those used here is the choice of $D = 0.20\ a_0^{-2}$, so that $w/a_0 \equiv 1/\sqrt{D} = \sqrt{5}$. The results from MQC calculations using FSSH[3b] (triangles connected by dotted lines) and MF-SD (boxes connected by lines) are shown in Figure 6, along with the exact results[3b] (grey circles connected by dotted lines). FSSH, MF-SD, and SPSH[3b] (not shown; see Fig. 4 of Ref. 3b), are numerically accurate for $k > 20$, and exhibit Stueckelberg oscillations, with MF-SD following the exact results to the lowest k among the three approximate methods. However, for $k < 15$, all three methods fail to obtain the correct amplitude and phase of the oscillations; the SPSH calculation in particular predicts a large unphysical discontinuity at $k \sim 13$. Thus, Figures 3 and 6 verify that w is sensitive to the range of the nonadiabatic coupling and is defined by the parameters of the system: in other words, the width of the frozen Gaussians is not a free parameter, but is instead system-defined.

We also studied the dual avoided crossing problem (Eqn. 26) as we changed the interaction width, w, while keeping the nonadiabatic coupling width fixed at $D = 0.06\ a_0^{-2}$ (for which Eqn. 24 suggests that w^2 should be about $16\ a_0^2$). Figure 7 gives the MF-SD results for a particle initially on the lower surface with $(w/a_0)^2 = 0.5$ (dash-dot curve), 4 (dashed curve), 16 (solid curve, same as Fig. 3a), and 128 (dotted curve). The exact results are shown as the solid grey circles (same as Fig. 3a). The most obvious deviation from the exact results is for $w^2 = 0.5\ a_0^2$. Moreover, although the transmission

probability for $w^2 = 128\ a_0^2$ appears identical to the result using $w^2 = 16\ a_0^2$, the choice of $w^2 = 128\ a_0^2$ incorrectly predicts no reflection on the lower surface. Hence, choosing w from the spatial extent of the nonadiabatic coupling to define the width of the frozen Gaussian wavepackets minimizes the deviation from the exact result, as we had determined empircally for the original three 1-D problems.

It is possible that the reason the nuclear width scales with this "interaction length" (the length over which the nonadiabatic coupling is strong) in these dual-avoided crossing examples is because decoherence should be defined by how a real nuclear wave packet experiences the crossings. For the original dual avoided crossing (Eqn. 26 and results presented in Fig. 3), the nonadiabatic coupling is significant over a range of at least 4 a_0, which spans both of the crossing events. Thus, the Gaussian wave packets need to be large enough to ensure interaction with both crossings before decoherence occurs. In the limit where the two crossings are infinitely far apart, the "interaction length" is only as wide as the nonadiabatic coupling is significant for each crossing. This leads to the question of how to find the "interaction length" in a complicated, condensed-phase calculation, where there is no simple diabatic formula for the nonadiabatic coupling. We will show in a subsequent article[20] that the width parameter, w, for condensed phase systems, is in fact readily available from simulation. Furthermore, we will show that for the hydrated electron, the average excited-state life time calculated by MF-SD is minimized by choosing the appropriate Gaussian width from the system-defined interaction width, providing the closest agreement with experiment.[20]

V. Concluding Remarks

When performing nonadiabatic mixed quantum/classical molecular dynamics, artificial methods for including decoherence are necessary because information about the total system wave function is lost when some degrees of freedom (the bath nuclei) are treated classically. In this paper, we introduced a new nonadiabatic MQC MD algorithm, called mean-field dynamics with stochastic decoherence (MF-SD), that allows the quantum subsystem to evolve into a superposition state but also includes a way for the superposition to decohere to a pure state. This process is irreversible in time and is controlled directly by the quantum/classical interaction through the Helmann-Feynman forces (Eqns. 8, 9, and 12). We used frozen Gaussians to approximate the nuclear wave function, and by expanding the nuclear wave function overlap (the decoherence function, Eqn. 10a) at short times, we obtained the nuclear-induced decoherence rate (Eqn. 12). In our algorithm, this rate determines the probability that the nuclear degrees of freedom should force the electronic superposition state to collapse into a pure state. Our method contains only one *ad hoc* parameter, which we have shown is not a free parameter but is instead defined by the system being studied.

We also have used a series of one-dimensional, two-state systems to show that MF-SD is at least

as quantitatively accurate as other popular MQC MD methods. MF-SD improves upon the accuracy of other MQC algorithms such as FSSH, SPSH, and MFSH for several reasons. First, MF-SD is built around a single, physically-motivated definition for decoherence, which we derived from arguments about the total system density matrix and the nature of nuclear wave function decay. Decoherence in our new algorithm is treated with only one criterion and the effects of decoherence on the quantum and classical systems are clearly defined: decoherence causes the quantum subystem to instantaneously collapse to a pure state, and the velocities of the particles in the classical subsystem are scaled in the direction of the effective nonadiabatic coupling vector to ensure energy conservation. Second, we use a mean-field description for the evolution of our quantum/classical system, which ensures that the dynamics calculated by MF-SD is governed by the TDSE and that a swarm of trajectories is not required. Third, MF-SD eliminates the need for a "reference" state, on which most MQC MD methods rely, and replaces it with a unified description of decoherence based on wave function collapse. This leads to improved accuracy when calculating quantum observables because elimination of the "reference" state ensures that weakly coupled quantum/classical systems remain in superposition states and do not undergo artificially imposed collapses back to the reference state. In addition to being more accurate, we also have argued that MF-SD is computationally more efficient than other popular nonadiabatic MQC MD simulation methods.

Acknowledgements

This work was supported by the National Science Foundation under grant number CHE-0204776. B.J.S. is a Camille Dreyfus Teacher-Scholar. We gratefully acknowledge UCLA's Academic Technology Services and the California Nanosystems Institute (CNSI) for the use of computational resources.

Appendix: Summary of Other Mixed Quantum/Classical Molecular Dynamics Algorithms

A. Fewest Switches Surface Hopping (FSSH)

In Tully's fewest switches surface hopping algorithm (FSSH; sometimes referred to as "molecular dynamics with electronic transitions," or MDET),[2] the classical particles propagate under the assumption that the quantum mechanical degrees of freedom occupy a single adiabatic state, j, called the reference state. Nonadiabatic transitions between states are modeled as instantaneous and discontinuous switches (surface hops) between the reference state and any other adiabatic state, k. The probability, P_{jk}, that the system should undergo a surface hop is governed by the rate of change of the elements of a fictitious[40] density matrix, via

$$P_{jk} = \frac{b_{kj}}{\rho_{jj}} dt \qquad \text{(A1)}$$

where *dt* is the simulation time step and

$$\dot{\rho}_{mm} = \sum_{l \neq m} b_{ml} = \sum_{l \neq m} \left[2\hbar^{-1} \mathrm{Im}\left(\rho_{ml}^{*} V_{ml}\right) - 2\,\mathrm{Re}\left(\rho_{ml}^{*} \mathbf{d}_{ml} \dot{\mathbf{R}} \right) \right] \tag{A2}$$

is the time rate of change of the m^{th} diagonal element of the fictitious density matrix; Eqn. A2 follows directly from the TDSE (Eqn. 5b).[2] In FSSH simulations, a surface hop occurs whenever the transition probability calculated from Eqn. A2 is greater than a random number chosen uniformly between zero and one. When a surface hop does occur, the discontinuous change in quantum energy is balanced by the kinetic energy of the bath, as described in Section III.B.2. The surface hopping check is performed on every time step, and the fictitious density matrix remains coherent for the entire trajectory; as a result, decoherence is not manifest in any individual trajectory. Coherence damping occurs only after adding together a swarm of trajectories from the same classical initial condition at the amplitude level. It is not clear, however, how many trajectories must be averaged in a swarm to properly account for decoherence, and the number of trajectories required almost certainly depends on the particular system under study. This need for a swarm of unknown size can add considerable computational cost. Recently, it was derived that detailed balance holds in FSSH calculations,[41] so that the populations of the quantum states are distributed according to the Boltzman distribution. It is not clear if other methods, including MF-SD, also have this advantage.

B. Stationary Phase Surface Hopping (SPSH)

In the stationary phase surface hopping algorithm (SPSH) introduced by Webster *et al.*,[3] the quantum subsystem is evolved fully coherently for each individual simulation time step, but at the end of each step, the system undergoes a collapse to one of the adiabatic basis states determined by the square of the transition amplitude,

$$P_{jk} = \left| \left\langle k(t) \middle| \hat{U}(t,t_0) \middle| j(t_0) \right\rangle \right|^2, \tag{A3}$$

where $\hat{U}(t,t_0)$ is the time evolution operator, $|j(t_0)\rangle$ is the occupied electronic state at the start of the time-step, and $|k(t)\rangle$ is any of the adiabatic electronic states at the end of the time step. We note that by performing a Taylor expansion of $\hat{U}(t,t_0)$, it is easy to show that P_{jk} in SPSH is identical to the surface hopping probability given in FSSH (Eqn. A1) in the limit that *dt* is infinitely small. The transition probabilities in SPSH are compared to a uniform random number, ξ, and a collapse is made to a new state *k* if $P_{jk} > \xi$, and to the original state *j* if none of the probabilities are greater than ξ. Thus, SPSH assumes that a measurement is made by the bath after every time step and that the quantum wave function is only coherent between time steps. Finally, in order to conserve energy during the fully coherent propagation

and collapse, the evolution of the mixed quantum/classical system is done using the Pechukas method,[31] which requires an iterative self-consistent evaluation of the quantum and classical dynamics. Modification of the SPSH algorithm to allow for decoherence times that are not linked to the simulation time step is challenging because the Pechukas force expression, which is derived from the stationary phase approximation, is non-local in time.[3b]

C. Mean Field Dynamics with Surface Hopping (MFSH)

The MFSH[4,5] algorithm allows for coherent mean-field propagation for short periods of time followed by full wave function collapse. MFSH uses the FSSH prescription for transitions between adiabatic states, and in doing so, requires two different density matrices for each MQC trajectory: a fictitious,[40] fully coherent "primary" density matrix, which keeps track of the FSSH transition probabilities, and an "auxiliary" density matrix, which is used to calculate the mean-field HF force.[42] Whenever a surface hop to state k is allowed, all the elements of the auxiliary density matrix are set to zero except ρ_{kk} which is set to 1. As with FSSH, the "primary" density matrix remains fully coherent throughout each trajectory. However, because the propagation of the auxiliary matrix produces dynamics that obeys the TDSE for short times, MFSH has the advantage that each MQC trajectory is physically meaningful. In addition to surface hops, MFSH treats coherence loss with "MF rescalings," where coherence in the electronic density matrix is destroyed and the mixed wave function is collapsed back to the "reference" state. This means that MFSH has two different but simultaneous definitions of decoherence, both of which cause unique responses in the quantum subsystem. Mean-field rescaling events are treated differently than surface hops because b_{kk} in Eqn. A2 is zero for all k; in other words, there is no nonadiabatic coupling vector (Eqn. 7) to induce a surface hop back to the reference state. The criteria for MF rescalings are determined by a second simultaneous MQC trajectory (called the "reference trajectory") that is computed along with the MFSH mean-field trajectory. The initial configuration and momenta in both trajectories are identical, but the classical particles in the reference trajectory experience the adiabatic HF force (Eqn. 9) from the reference state, while the classical particles in the mean-field trajectory experience the mean-field HF force (Eqn. 8); the two trajectories eventually diverge in the presence of any nonadiabatic coupling. MFSH compares the two trajectories and allows for wave function collapse to the reference state when they have diverged sufficiently; this is taken to be whenever either of the inequalities

$$\left|\frac{P_{MF} - P_{ref}}{P_{MF} + P_{ref}}\right| << 1 \tag{A4}$$

$$\left|R_{MF} - R_{ref}\right| << a_0 \tag{A5}$$

is violated for any classical particle, where P_{MF} (R_{MF}) and P_{ref} (R_{ref}) are the classical momenta (positions) in the MF and reference trajectories, respectively. When either of the inequalities A4 or A5 is violated, the "auxiliary" density matrix is reset so that the quantum wave function in the mean-field trajectory collapses to the reference state and the classical coordinates in the reference trajectory are reset to match the MF trajectory, although the primary density matrix is not reset (the reference trajectory coordinates are reset if a surface hop or MF rescaling occurs). Finally, as in FSSH, to ensure conservation of energy, surface hops require the classical velocities to be scaled along the direction of the NA coupling vector, whereas MF rescalings require the classical velocities to be scaled along the direction of the effective nonadiabatic coupling vector (Eqn. 20).[5]

Two modifications of MFSH have been presented in the literature: the average decoherence (ad-)[18] and instantaneous decoherence (id-)[19] with MFSH algorithms. In both id-MFSH and ad-MFSH, the off-diagonal elements of the "auxiliary" and "primary" density matrices are dissipated according to

$$i\hbar \frac{d}{dt}\rho_{kj} = \sum_n \sum_l \left[\rho_{lj}\left(V_{kl} - i\hbar \mathbf{d}_{kl}^n \cdot \dot{\mathbf{R}}_n \right) - \rho_{kl}\left(V_{lj} - i\hbar \mathbf{d}_{lj}^n \cdot \dot{\mathbf{R}}_n \right) \right] - i\hbar \frac{(1-\delta_{kj})\rho_{kj}}{\tau_{kj}} \qquad \text{(A6)}$$

where the Kronecker delta in the last term ensures that the dissipation affects only the off-diagonal elements (*cf.* Eqn. 5b). In Eqn. A6, the decoherence time τ_{kj} represents coherence loss between two adiabatic states, k and j, which can either be pre-determined and thus fixed throughout the entire simulation, ad-MFSH, or be calculated instantaneously for each configuration, id-MFSH. Both modifications are identical in all other ways to the original MFSH algorithm, which is recovered in the limit $\tau_{kj} \to \infty$.

D. Full Multiple Spawning (FMS)

The full multiple spawning (FMS) method, developed by Martinez and co-workers,[6] uses the frozen Gaussian approximation and the equations of motion derived by Heller[25] to represent the nuclear wave function. The total wave function of the system, Ψ, is described as a linear combination of basis functions, ψ_i (with expansion coefficients, D_i) that are products of a nuclear wave function and a set of orthonormal electronic basis states. The coefficients evolve according to the TDSE, and the method involves propagating a set of carefully chosen starting configurations, each of which starts with only one basis function. Whenever a trajectory enters a region of strong nonadiabatic coupling, new basis functions are "spawned" on the coupled electronic states, representing the population changes predicted by the TDSE. The spawned basis functions can in turn create spawns of their own as they enter additional regions of strong nonadiabatic coupling. The idea of introducing new basis functions is to allow the total wave function to bifurcate as a real quantum wave function should. Final state populations and

observables are calculated after all spawns have escaped all regions of non-adiabatic coupling using the coefficients, D_i, in the linear combination of basis functions. The spawned trajectories are typically chosen to preserve the total classical energy, as well as either the classical positions or classical momentum. Momentum-conserving spawns have the advantage of allowing for tunneling of the nuclei, which is impossible for most other MQC MD methods. Although FMS requires significant computational effort, it has found utility as an *ab initio* MD method for fairly large molecules, including small proteins, in the gas phase.[43] In the condensed phase, FMS has thus far found utility as a QM/MM method[44] in which the electronic structure in the subsystem treated by FMS does not directly influence the classical bath.

E. Self-Consistent Decay of Mixing (SCDM)

The self-consistent decay of mixing (SCDM) algorithm of Truhlar and co-workers[7] incorporates a term in the TDSE for coherence loss in the off-diagonal elements of the density matrix, but unlike the ad- and id-MFSH methods, SCDM adds the innovation of supplementary terms in the classical equations of motion and the diagonal density matrix elements. These extra terms attempt to model decoherence by continuously and smoothly driving the mean-field wave function in an SCDM trajectory towards a single adiabatic reference state while conserving energy and angular momentum, and ensuring $\mathrm{Tr}(\rho) = 1$. SCDM uses the FSSH probabilities to determine the reference state, however, the modified SCDM equations of motion allow these surface hopping events to occur over a finite time rather than instantaneously. This might be a more accurate treatment of coherence loss than instantaneous wave function collapse and has the advantage of trajectories that never undergo discontinuous changes in the quantum wave function or density matrix. As a result, there are no energy conservation problems in SCDM that might lead to a "forbidden" transition; see Section III.B.2. SCDM has the drawback, however, that there is no easy prescription to derive the decoherence and population decay times used in integrating the equations of motion: in the original SCDM algorithm, the authors included an arbitrary scaling factor so the decoherence time could be adjusted at will; in a recent paper, however, Jasper and Truhlar have derived a first-order decoherence rate from a formula similar to Eqn. 10b.[33] In addition, because SCDM uses the FSSH probabilities, SCDM trajectories will always necessarily end in a pure state, even when the classical and quantum subsystems are no longer interacting. We have arged that in such cases, the quantum subsystem could end up in a superposition state, but SCDM cannot predict this properly (e.g., the extended coupling problem discussed in Section IV.C).

Table Caption:

Table I – Comparison of features of the new algorithm introduced in this paper, MF-SD, to four other nonadiabatic mixed quantum/classical algorithms that are summarized in the Appendix. In each entry, MF abbreviates "mean-field"; MQC abbreviates "mixed quantum/classical", and MD abbreviates "molecular dynamics."

Figure Captions:

Figure 1 – Adiabatic Surfaces for Two-Level Model Problems: The adiabatic energy levels as a function of position for the (a) single avoided crossing, (b) the dual avoided crossing, and (c) the extended coupling model problems. The diabatic Hamiltonians that describe these three problems are taken from Tully in Ref. 2 and given explicitly in Eqns. 25, 26 and 28, respectively.

Figure 2 – Single Avoided Crossing: (a) Probability for transmission on the lower adiabatic state, (b) probability for transmission on the upper adiabatic state and (c) probability for reflection on the lower adiabatic state for the model potential given by Eqn. 25 whose adiabatic surfaces are shown in Fig. 1a. The MF-SD results are the solid boxes connected by lines, the FSSH results[2] are the open grey triangles, and the exact results[2] are the open grey circles;[36] two-standard-deviation error bars are smaller than the symbols used to represent the MF-SD data points.

Figure 3 – Dual Avoided Crossing: (a) Probability for transmission on the lower adiabatic state, (b) probability for transmission on the upper adiabatic state and (c) probability for reflection on the lower adiabatic state for the model potential given by Eqn. 26 whose adiabatic surfaces are plotted in Fig. 1b. The MF-SD results are the solid boxes connected by lines, the FSSH results[2] are the downward facing triangles, the MFSH results[4] are the exes, and the exact results[4] are the solid grey circles;[36] the two-standard-deviation error bars are smaller than the symbols used to represent the MF-SD data points. The FSSH results for transmission, shown in Fig. 5 of Ref. 2, are omitted here for clarity; they are nearly identical to the MFSH and MF-SD transmission probabilities.

Figure 4 – Transition Probabilities for Dual Avoided Crossing: Probability for an upward transition for a fully adiabatic, ground state trajectory with initial momentum k = 14.14 a.u. ($log(E/\text{a.u.}) = -3$). The *minimum* transition probability from an FSSH trajectory (dotted curve) is given by Eqn. 27a, and the *maximum* transition probability an MF-SD trajectory (solid curve) is given by Eqn. 27b (see text); to better compare the two curves, the maximum MF-SD probability curve is multiplied by 20. The dashed-

grey curves are the adiabatic surfaces for the dual avoided crossing, reproduced and scaled here for reference.

Figure 5 – Extended Coupling: (a) Probability for transmission on the lower adiabatic state, (b) probability for reflection on the lower adiabatic state and (c) probability for reflection on the upper adiabatic state for the model potential given by Eqn. 28 whose adiabatic surfaces are shown in Fig. 1c. The symbols have the same meanings as in Fig. 3.[36] The MFSH results are not shown in panel (a) because they are indistinguishable from the exact results. In panels (b) and (c), the MFSH data points are connected by lines to better show the spurious oscillations in the reflection probabilities.[38]

Figure 6 – Narrow Dual Avoided Crossing: Survival probability on the upper adiabatic state of the dual avoided crossing the problem defined in Eqn. 26 but with D = 0.2 a_0^{-2} instead of 0.06 a_0^{-2}. The MF-SD results are the boxes connected by solid lines, the FSSH results[3b] are the triangles connected by dotted lines, and the exact results[3a] are the grey circles connected by dotted lines;[36] the SPSH results can be found in Figure 4 of Ref. 3b.

Figure 7 – Effect of the Interaction Width in the Dual Avoided Crossing: Variation of the lower-surface transmission (a) and reflection (b) with the interaction width, w, Eqn. 24 for the dual avoided crossing problem described by Eqn. 27. Results are shown for $w^2/a_0^2 = 0.5$ (dashed curve), 4 (grey dashed curve), 16 (solid curve, same as the data in Figs. 3a and 3c), 128 (dotted curve), and the exact results[4] (grey boxes, same as in Figs. 3a and 3c).[36] Error bars are two standard deviations; for clarity, the error bars are not shown for every data point. The curve for $w^2 = 128$ is not visible in panel (a) since it lies exactly on top of the curve for $w^2 = 16$.

References:

1 *Classical and Quantum Dynamics in Condensed Phase Simulations*, edited by B. J. Berne, G. Ciccotti, and D. F. Coker (World Scientific, Singapore, 1998).

2 J. C. Tully, J. Chem. Phys. **93**(2), 1061 (1990).

3 (a) F. Webster P. J. Rossky, and R. A. Friesner, Comp. Phys. Comm, **63**, 494 (1991). (b) F. Webster, E. T. Wang, P. J. Rossky, and R. A. Friesner, J. Chem. Phys. **100** (7), 4835 (1994)

4 O. V. Prezhdo, and P. J. Rossky, J. Chem. Phys. **107** (3), 825 (1997).

5 K. F. Wong, and P. J. Rossky, J. Phys. Chem. A **105**, 2547 (2001).

6 (a) T. J. Martinez, M. Ben-Nun, and R. D. Levine, J. Phys. Chem. **100**, 7884 (1996). (b) M. Ben-Nun and T. J. Martinez, J. Chem. Phys. **112** (14), 6113 (2000). (c) T. J. Martinez, M. Ben-Nun, and R. D. Levine J. Phys. Chem. **100**, 7884 (1996).

7 (a) M. D. Hack, and D. G. Truhlar, J. Chem. Phys. **114** (21), 9305 (2001). (b) C. Y. Zhu, A. W. Jasper, and D. G. Truhlar, J. Chem. Phys. **120** (12), 5543 (2004). (c) C. Y. Zhu, S. Nangia, A. W. Jasper, and D. G. Truhlar, J. Chem. Phys. **121** (16), 7658 (2004).

8 (a) C. C. Martens and J.-Y. Fang, J. Chem. Phys. **106** (12), 4198 (1997). (b) A. Donoso and C. C. Martens, J. Chem. Phys. **112** (9), 3980 (2000).

9 R. Car, and M. Parrinello, Phys. Rev. Lett. **55**, 2471 (1985).

10 J. C. Tully, and R. K. Preston, J. Chem. Phys. **55**, 562 (1971).

11 (a) D. F. Coker and L. Xiao, J. Chem. Phys. **102** (1), 496 (1995). (b) V. S. Batista and D. F. Coker, J. Chem. Phys. **105** (10), 4033 (1996).

12 E. Schrödinger, Translated by J. D. Trimmer, Proc. of the Phil. Soc., **124**, 323 (1980).

13 J. von Neumann, originally chapters V and VI of *Mathematische Grundlagen der Quantenmechanik*, pp. 184-237 (Springer, Berlin 1932). Translation English by R. T. Beyer, *Mathematical Foundations of Quantum Mechanics*, pp. 347-445 (Princeton University Press, Princeton, 1955).

14 W. H. Zurek, Phys. Today **44** (10), 36 (1991).

15 S. Mukamel, *Principles of Nonlinear Optical Spectroscopy*, Oxford University Press (New York, NY, 1995)

16 This form of Eqn. 2 assumes that we have projected onto a slightly unusual set of product basis functions, $\{(|\phi_k\rangle|\chi_k\rangle)_k\}$, where the last subscript means that each product in this set is propagated under the influence of *adiabatic* electronic state k. The elements of the density matrix operator

in Eqn. 1, in contrast, are propagated via the TDSE under the influence of the electronic superposition, or mean field (MF) state. This means that when we project the density matrix operator (Eqn. 1, with indices *j*) onto the basis set of adiabatically propagated states (denoted by indices *k*), we obtain inner products consisting of overlaps between mean-field and adiabatic basis states. These overlaps have the form $\sum_j c_j^* \,{}_{MF}\langle \phi_{j'} | \phi_k \rangle_k \approx c_k^* \delta_{j'k}$, where the subscript *MF* denotes propagation under the influence of the electronic superposition (mean-field) state and the approximate equality holds at short times when there has been no significant electronic decoherence. Because our new method relies on a short-time approximation and neglects electronic decoherence, as discussed in Section III, we make use of the short-time approximate equality in our definition of the decoherence function.

17 This approximation should be valid in the condensed phase because MQC MD simulations typically deal with hundreds or thousands of classical degrees of freedom and only one or two quantal degrees of freedom. Since the simulation time step is usually chosen to accurately integrate the quantum motions, the associated quantum degrees of freedom do not change much from one time step to the next, leading to little change in the electronic density matrix. The nuclear decoherence function, however, depends on the collective overlap of *all* the classical particles; if even a single classical particle loses phase, then the entire $D_k(t)$ goes to zero.

18 K. F. Wong and P. J. Rossky J. Chem. Phys. **116** (19), 8418 (2002).

19 K. F. Wong and P. J. Rossky J. Chem. Phys. **116** (19), 8429 (2002).

20 R. E. Larsen, M. J. Bedard-Hearn, and B. J. Schwartz, manuscript in preparation.

21 We note that one of the most popular MQC MD methods, Tully's fewest switches surface hopping algorithm (Ref. 2), uses a swarm of trajectories to calculate quantum observables because the dynamics of individual trajectories in the method are not physically significant.

22 As a practical point, the option of using diabatic basis sets in the condensed phase is often not a possibility without extensive computational cost; see, e.g., R. J. Cave and M. D. Newton, Chem. Phys. Lett. **249** (1-2), 15 (1996).

23 K. Drukker, J. Comput. Phys. **153**, 225 (1999).

24 (a) E. Neria, A. Nitzan, R. N. Barnett, U. Landmann Phys. Rev. Lett. **67**, 1011 (1991). (b) E. Neria, A. Nitzan J. Chem. Phys. **99** (2) 1109 (1993). (c) E. Neria, A. Nitzan Chem. Phys. **183**, 351 (1994).

25 E. J. Heller, J. Chem. Phys. **75**, 2923 (1981).

26 B. J. Schwartz, E. R. Bittner, O. V. Prezhdo, and P. J. Rossky *J. Chem. Phys.* **104** (15), 5942 (1996).

27 MF-SD calculates how likely it is for nuclear phase to be lost only over the next finite time step of the MD simulation, dt. Since simulation time steps are chosen to be extremely short in order to prevent the electronic wave function from changing drastically between time steps, this allows us to safely invoke the Taylor expansion for the decoherence of the nuclear wave function, $D_k(t)$, between t and $t+dt$. The frozen Gaussian approximation is appropriate because we assume that the quantum nature of the classical subsystem is fully coherent at the beginning of each time step; that is, if we knew the entire nuclear wave function at the beginning of each simulation time step, it would be fully coherent. Since we are only concerned with $D_k(t)$ for a short length of time, dt, it is safe to assume that the Gaussians will not spread during that time interval.

28 This discontinuity means that MF-SD is not a time-reversible algorithm, which is consistent with von Neumann's "Process I." (Ref. 13)

29 S. Hammes-Schiffer and J. C. Tully, J. Chem. Phys. **101** (6), 4657 (1994).

30 U. Müller and G. Stock, J. Chem. Phys. **107** (16), 6230 (1997).

31 P. Pechukas, Phys. Rev. **181**, 174 (1969).

32 The frozen Gaussian and short-time approximations that we make for MF-SD might not apply in all condensed-phase systems. In glasses and solids, for example, the rate of electronic decoherence is likely to occur on the same time-scale as nuclear-induced decoherence – that is, the off diagonal elements of the electronic density matrix may be decaying at the same rate as $D_k(t)$ (see Eqn. 2).

33 A. W. Jasper and D. G. Truhlar, J. Chem. Phys. **123** 064103 (2005).

34 W. H. Press, S. A. Teukolsky, W. T. Vetterling and B. P. Flannery, *Numerical Recipes in C: The Art of Scientific Computing,, Second Edition* (Cambridge University Press, New York, NY, 1999).

35 For the extend coupling problem in reflection, all of the initial momenta we use are greater than the energy gap, which is $1.2\text{x}10^{-3}$ Hartree

36 The data used in these figures were taken from published figures. A program called DigitizeIt (www.digitizeit.de) was used to extract the data from digitally reproduced copies of the cited articles. Selection of the data points was reproducible to within ~1%, which is smaller than the size of the symbols used to represent them in this article.

37 Note that when $\mathbf{v}\bullet\mathbf{d}_{12} < 0$, $P_{\text{FSSH}} = 0$

38 Not shown in Fig. 5a is the MFSH result for transmission on the upper surface, because the results are numerically exact with no artificial oscillations. In addition, FSSH shows the same false oscillations as

MFSH in the reflection probabilities, but their magnitude is much larger than MFSH; see Fig. 6 of Ref. 2.

39 Of course, FSSH methods obtain the transmission probabilities correctly for this problem because there is no nonadiabatic coupling to the right of $x = 0$ to induce incorrect decoherence events.

40 The density matrix is "fictitious" because the superposition it describes does not interact with the classical subsystem in any way; it is only a book-keeping device for the FSSH algorithm.

41 (a) P. V. Parandekar and J. C. Tully, J. Chem. Phys. **122** (9), 094102 (2005). (b) R. E. Larsen, P. V. Parandekar and J. C. Tully, *in preparation.*

42 The definition of "primary" and "auxiliary" switches between Refs. 4 and 5; in this paper, we use the convention presented in Ref. 5.

43 K. K. Baeck and T. J. Martinez, Chem. Phys. Lett. **375**, 299 (2003).

44 (a) A. Toniolo, G. Granucci, and T. J. Martinez , J. Phys. Chem. A. **107**, 3822 (2003). (b) A. Toniolo, S. Olsen, L. Manohar, and T. J. Martinez, Faraday Discuss. **127**, 149 (2004).

Algorithm	Decoherence Methods	Surface Switching	Comments
FSSH[2]	Adiabatic trajectories; Check for surface hops after every time step; Swarm of trajectories required; Observables from averages of the "reference state"	Fully coherent propagation of "fictitious" density matrix for each trajectory; Coherence is lost only after the swarm is averaged	Based on the rate of change of diagonal elements of the "fictitious" density matrix, Eqn. A1	Avoids chatter between states that are no longer coupled, unlike older surface hopping methods (e.g., Ref. 10)
SPSH[3]	Self-consistent propagation with the Pechukas method; Observables calculated from averages of the "reference state"	Fully collapse the wave function to an adiabatic state after every simulation time step	Transition probabilities between adiabatic states based on overlap between two states before and after the simulation time step, Eqn. A3	Coherent evolution of the classical and quantum particles, only for short periods of time; Pechukas force is non-local in time
MFSH[4]	Requires both a MF trajectory and a reference trajectory and both real and "fictitious" density matrices; Observables calculated from averages of the "reference state"	Density matrix remains coherent until surface hop or MF rescaling occurs; MF rescale when mean-field and reference trajectories diverge, Eqns. A4 & A5	Same as FSSH; Check for SH or possible MF rescaling after every simulation time-step	MF dynamics without self-consistent forces, but requires 2 MQC trajectories to be run simultaneously; id- and ad- versions also damp quantum phase
FMS[6]	One semi-classical trajectory spawns new trajectories whenever the nonadiabatic coupling strength is large; Observables calculated from density matrix	Treatment of nuclear wavefunction as frozen Gaussians leads to realistic decoherence	Multiple spawns on all of the coupled electronic states allow for bifrucation of electronic and nuclear wave functions	Useful as an ab initio MD method; Allows for tunneling; Very expensive for condensed-phase applications
MF-SD (this work)	One MQC trajectory; Stochastic collapse of the MF wave function based on nuclear-induced decoherence; Observables from density matrix	Total wave function collapse between superposition state and adiabatic pure state, Eqn. 13, based on nuclear dynamics	Decoherence induces collapse of the MF wavefunction to a pure state, which may or may not be different than the original state	Lack of "reference" trajectory improves efficiency; Decoherence & surface hops treated equally; Accuracy improved in 1-D examples

Table I - M. J. Bedard-Hearn, et. al.; Submitted to J. Chem. Phys.

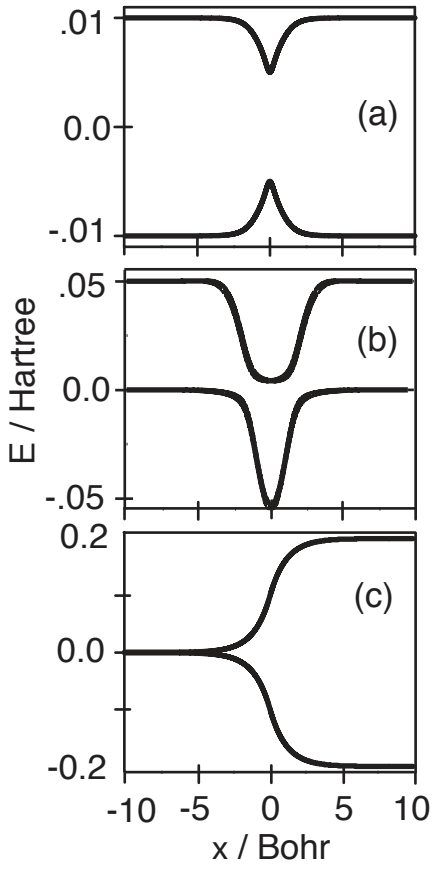

Figure 1 - M. J. Bedard-Hearn, et. al.; Submitted to J. Chem. Phys.

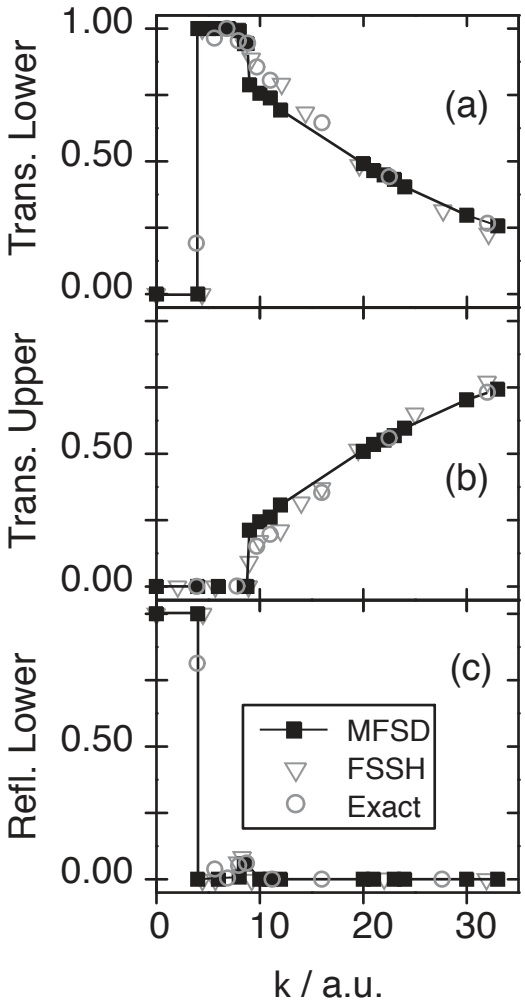

Figure 2 - M. J. Bedard-Hearn, et. al.; Submitted to J. Chem. Phys.

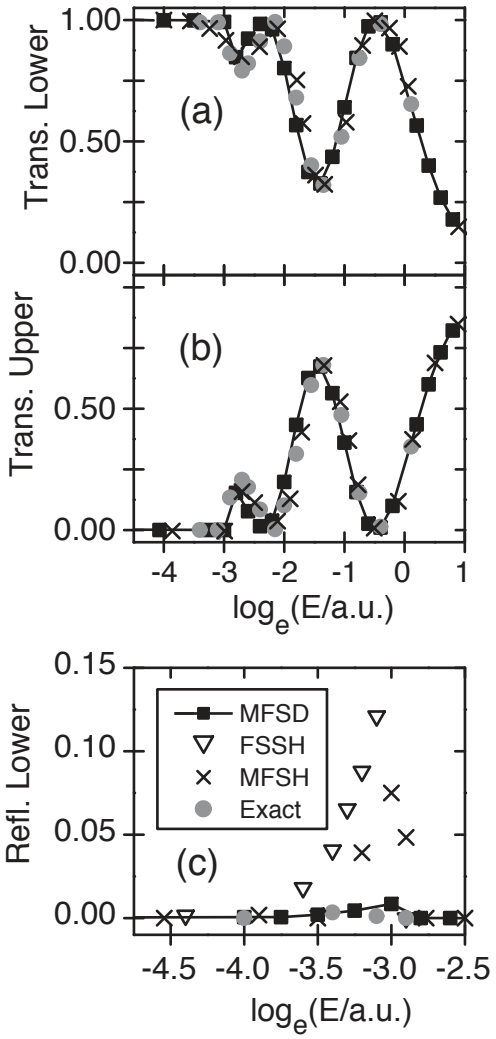

Figure 3 - M. J. Bedard-Hearn, et. al.; Submitted to J. Chem. Phys.

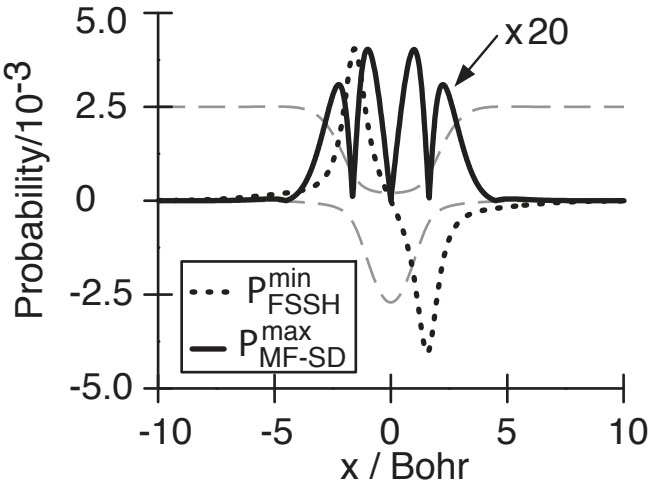

Figure 4 - M. J. Bedard-Hearn, et. al.; Submitted to J. Chem. Phys.

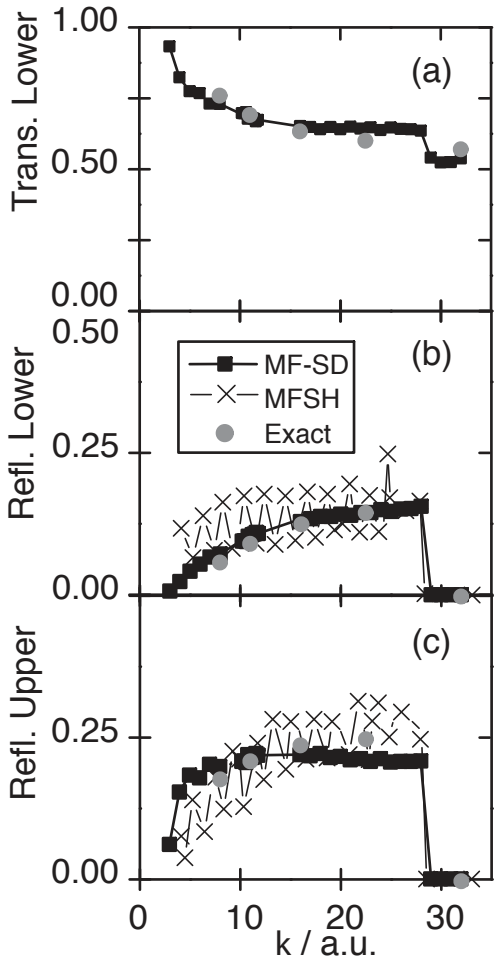

Figure 5 - M. J. Bedard-Hearn, et. al.; Submitted to J. Chem. Phys.

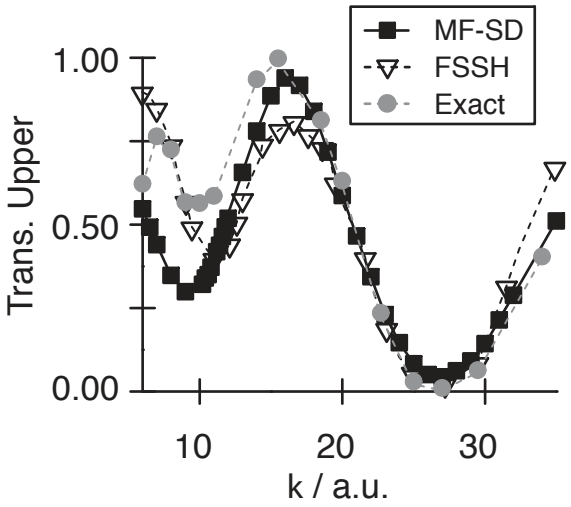

Figure 6 - M. J. Bedard-Hearn, et. al.; Submitted to J. Chem. Phys.

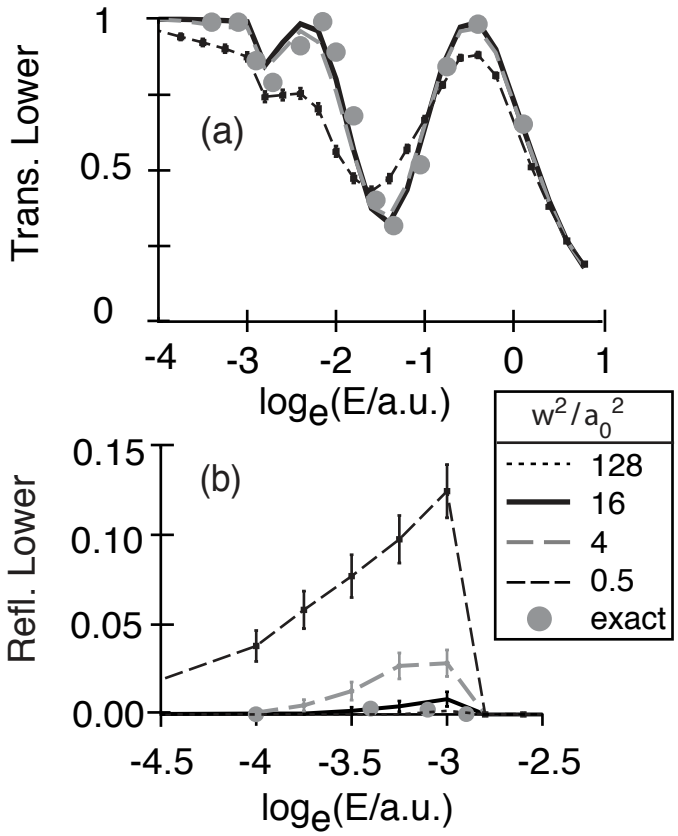

Figure 7 - M. J. Bedard-Hearn, et. al.; Submitted to J. Chem. Phys.